Modelling ocean wave conditions at a shallow coast under scarce data availability – A case study at the western coast of the Mekong Delta, Vietnam

Moritz Zemann[1,2], Roderick van der Linden[3], Trinh Cong Dan[1], Duong Hoang Thai Vu[1], Nguyet Minh Nguyen[4], Frank Seidel[1], Peter Oberle[1], Franz Nestmann[1], Andreas H. Fink[3]

[1]Karlsruher Institut of Technology, Institute of Water and River Basin Management, Hydraulic Engineering and Water Resources Management, Kaiserallee 12, 76131 Karlsruhe
[2]Disy Informationssysteme GmbH, Ludwig-Erhard-Allee 6, 76131 Karlsruhe
[3]Karlsruher Institut of Technology, Institute of Meteorology and Climate Research, Kaiserallee 12, 76131 Karlsruhe
[4]Souther Institute of Water Ressources Research (SIWRR), Q.5, 658 Đ. Võ Văn Kiệt, Phường 1, Quận 5, Thành phố Hồ Chí Minh, Vietnam

Correspondence to: Moritz Zemann (moritz.zemann@gmx.de)

Abstract: Against the background of the rising sea level and land subsidence, protecting the progressively eroding coast along the Vietnam Mekong Delta becomes of tremendous importance. Within the presented work, design conditions for breakwaters were derived from offshore climate reanalysis data (ERA5), which were transferred to the nearshore by two numerical approaches, i.e. SwanOne and Delft3D, for different average and extreme wave and weather conditions. Within this process, design wave heights and periods at the nearshore could be determined for 10- to 100-year recurrence intervals. Both models thereby showed sufficient accuracy according to measurements in the field. Limitations must be made regarding the available spatio-temporal resolution, where reanalysis data showed a lack of short but high peak values compared to the observed measurements. Both numerical approaches showed their capabilities, where SwanOne offers a simple and fast calculation method, while it lacks of continuous effects like wind-generated swell or bottom friction. The Delft3D software on the other hand provides a more complete representation, not only of wave but also current dynamics, while it requires a much broader amount of input parameters and more complex boundary conditions. Within this study, the advantages and disadvantages of both models could be demonstrated, whereas for the final calculation of nearshore wave characteristics, only SwanOne was applicable based on the input parameters extracted from statistical analysis of long term ERA5 data.

1 Introduction

The Mekong Delta (MD) is located at the southern part of Vietnam (see Figure 1). It is characterised by two coastlines: One along the Gulf of Thailand (lokally known as the West Sea) and the other towards the South China Sea (locally known as East Sea). Concerning the economy of Vietnam, the MD is most important for agricultural production (rice, shrimps) and exporting goods (The Anh et al. 2020; Vu et al. 2021). However, during the last decades, the coastline around the MD experienced severe degradation (Allison et al. 2017; Marchesiello et al. 2019; Lappe et al. 2022). Comparison of results from remote sensing between 2003 and 2012 showed that 68% of the shoreline experienced erosion (Besset et al. 2019). Land subsidence processes, as a result of groundwater over-abstraction, combined with climate change induced sea level rise might add up to a serious threat over the upcoming decades, especially since the whole Delta is situated on average only around 0.8 m above the sea level (Minderhoud et al. 2019). Further pressure arises from existing and projected upstream dams along the Mekong river, with its negative impact on the deltaic sediment balance (Allison et al. 2017; Bussi et al. 2021). In addition, the sediment balance is as well heavily influenced by sand mining activities in the main rivers (Jordan et al. 2019; Franca et al. 2022). Against the background of the described pressures and the political intention to sustainably develop this important region, the stop of further erosion along with the goal of stabilizing the coastline by land reclamation and mangrove replantation is defined as an urgent task for the MD (Chu Van Cuong et al. 2015).

In this context, the construction of detached breakwater would offer the possibility to prevent further coastal erosion as well as enhance soil deposition and land reclamation behind the breakwaters. Various breakwater types, i.e. pile-rock breakwaters (Le Xuan et al. 2020), precast hollow concrete breakwaters (Dao et al. 2021; Le Xuan et al. 2022), bamboo fences (Dao et al. 2021), and curtain wall breakwaters (Vu et al. 2022) had been studied or already implemented along the coast to investigate their suitability under the local conditions with hit-and-miss (Nguyen et al. 2020). Successful examples, like the pile-rock breakwaters, featuring three-meter distant concrete pillar rows filled with rocks, showed promising results within the last years in terms of erosion control and land reclammation (Groenewold and Peters 2016). However, these structures require massive amounts of construction materials (i.e. rocks) which are not naturally available in the region and therefore need to be transported from far distance. Malfunction of structures was often linked to missing information on, e.g. about foundation conditions or extreme sea state statistics (Nguyen et al. 2020). According to the huge extent of the MD coastline, sophisticated and specific approaches of coastal protection become more and more important (Albers and Schmitt 2015).

To warrant the intended performance and the structural stability of a breakwater over its design lifetime, the knowledge of average and extreme sea states in terms of design conditions is of crucial importance to the planning process. Here, the availability of long-term measured data in the area reveals huge gaps. Data assessment close to the coast, which would be the area of breakwater construction, was ofthen performed only for short periods ranging from single measurements up to discontinuos measurements spread over a few weeks (Albers and Stolzenwald 2014; Marchesiello et al. 2018), therefore neglecting extreme weather events during the year.

The whole region is characterized by a wet and dry monsoon with winds from the southwest and northeast, respectively (compare **Figure 1**), which cause shifting patterns of waves and currents around the Cape Ca Mau and lead to substantial erosion and accretion of the fine sediments that make up the Delta. The summer monsoon lasting approximately from May to early October is characterized by high precipitations rates (Allison et al. 2017). The dominant wind and wave direction is south-westerly during the summer monsoon (Thoai et al. 2019; Albers and Stolzenwald 2014). During this season, there is a strong sediment transport into the northeast direction along the western coast (Le Tu et al. 2019). In contrast, the winter monsoon takes place from November to early March (Unverricht et al. 2014) and features low precipitation rates but higher average wind speeds than during summer monsoon (Thoai et al. 2019). Winds and waves are approaching mainly from a northeastern direction during the winter monsoon (Unverricht et al. 2014). The longshore current during the winter monsoon is mainly following a southwestern direction (Nguyen et al. 2022). Currents thereby show maximum speeds of up to 0.7 m s^{-1}. However, these velocities show little influence from the monsoon (Albers et al. 2013). Tidal conditions are also strongly depending on the location (**Figure 1**). The western coast experiences tidal ranges of around 0.8 m – 1 m, while the eastern coastline shows much greater tidal ranges of 1 m – 3 m (Albers and Stolzenwald 2014).
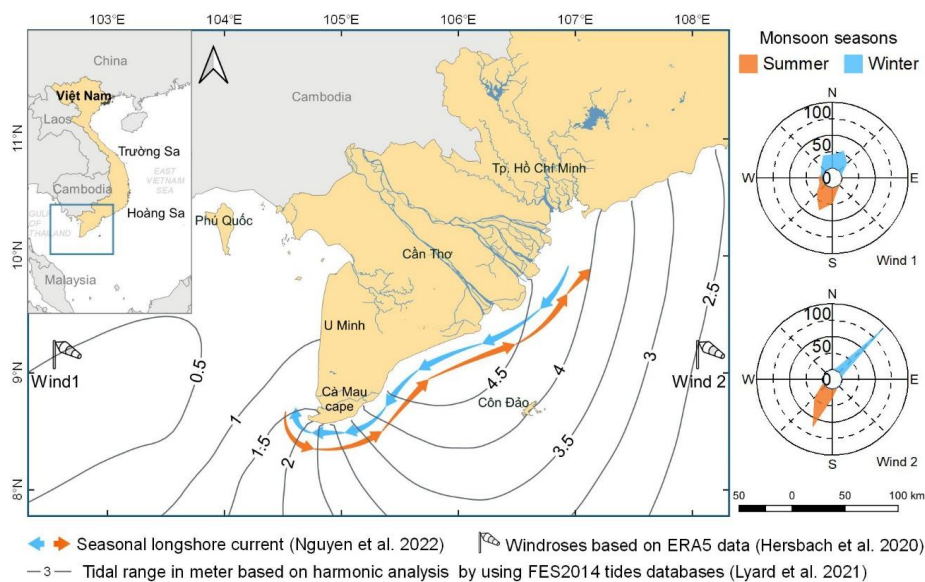
Figure 1: Schematic overview of tides, currents and wind characteristics around the Mekong Delta during Summer and Winter monsoon.

76   The coastal bathymetry in the western coast of the MD is very shallow and characterised by gradually increasing
77   slopes ranging only between 1:600 up to 1:1200 for more than 10 km out to sea (see **Figure 2**) Whilst the depth
78   profile of the coastline varies along the delta, the area around the cape Ca Mau is especially flat (Nguyen Trung
79   Thanh et al. 2017).

80   Short term wave measurements over 15 days with a distance of 14 km to the West coast in U Minh district (see
81   **Figure 1**) showed maximum significant wave heights of 1.6 m (mean of 0.9 m) from October to November, while
82   wave heights reduce to 0.6 m (mean 0.3 m) from February to March, demonstrating the rather calm conditions
83   during the winter monsoon. Maximum wave heights reached up to 2.4 m (maximum) and 1.3 m (mean) during
84   late summer and 1.0 m (maximum) and 0.5 m (mean) during winter (Marchesiello et al. 2017). Average wave
85   periods followed a similar pattern with longer periods corresponding to greater wave heights, which fell in the
86   range of 5.5 s for the eastern coast during the northeast monsoon, and 3.5 s at the western coast during the
87   southwest monsoon (Marchesiello et al. 2017).

88   In comparison to such short-term measurements, long-term data are only available from national stations in
89   distances far away to the relevant coast (e.g. Phu Quoc island, see **Figure 1**). Remote sensing data from satellites
90   ofthen feature high uncertainties and are difficult to calibrate. More accurate climate reanalyses like ERA5
91   (ECMWF Reanalysis 5) do not consider the relevant areas close to the coast as they typically start with around
92   10 km distance and comprise rather coarse grid resolution of 0.5°, which approximately equals to 55 km for the
93   MD are. The latest local seadyke regulations were as well aware of the scarce data availability and therefore
94   suggest modelling simulations to increase the reliability of oceanographical data (MARD 2012).

95   Against this background, the main aim of this study is to determine extreme wave conditions to support the
96   dimensioning of nearshore breakwaters.Therefore statistically analized long-term offshore data (wave & wind)
97   from a climate reanalysis (ERA5) are verified by onsite measurements. Within the framework of a field campaign
98   in July 2019, wave data were measured offshore and nearshore over a two week period. Within a modell approach,
99   the third-generation wave model SWAN (Simulating Waves Nearshore) was applied to simulate wave propagation
100   from offshore to nearshore using the 1D linear approach featured by SwanOne and the 2D spatial approach featured
101   by Delft3D-WAVE. ERA5 data during the measurement campaign were thereby used as model input to validated
102   with the on-site measurements. Afterwards statistical long-term data for average and extreme conditions from 40-
103   year ERA5 time series were used as input to determine the site-specific design conditions. Besides, a comparison

104   of SwanOne and Delft3D was performed for a eight day lasting storm event in 2000, to assess their overall
105   applicability, reliability, and limitations under different conditions.

106   SwanOne and Delft3D-WAVE have been applied in various studies (Duy Vinh et al. 2016, Le Tu et al. 2019,
107   Thanh et al. 2017, Tas 2016) for the MD and demonstrated their capability in reproducing coastal wave heights,
108   currents and sediment transport. Delft3D-FLOW was used in a coupled approach with Delft3D-WAVE to
109   investigate seasonal sedimentation distribution around the Mekong coast. (Duy Vinh et al. 2016) applied it
110   successfully to investigate the interaction of increasing wave heights and sediment resuspension. Another coupling
111   of the Delft3D-FLOW and the Delft3D-WAVE model investigated the Mekong estuaries' morphodynamics under
112   influence of salinity, tide and wind (Le Tu et al. 2019). A combination of the large-scale hydrodynamic model
113   (Delft-FM) and a small-scale model (Delft3D-4 Suite) was used to study sedimentation in the Mekong estuaries
114   due to seasonal forces and coastal processes (Thanh et al. 2017).

115   Tas (2016) applied SwanOne to transfer offshore boundary conditions in the MD to nearshore, which then were
116   further used as input for SWASH (Simulating Waves till Shore), a phase-resolving wave model to further
117   investigate wave dynamics as they were running up shore. Transfer of ECMWF ERA-40 offshore waves towards
118   the nearshore had been performed using SWAN for the eastern mainland coast, to quantify the effects of climate
119   change to wave characteristics and longshore sediment transport. However, the western coast of the MD was not
120   considered within this study (Dastgheib et al. 2016). Further applications of SwanOne were utilized for predicting
121   nearshore waves (Huong 2003), for storm generated wave simulation (Hoque et al. 2020), for validation of wave
122   transfer for physical experiments (Herrera et al. 2017), and for shallow water wave modelling (Moghimi et al.
123   2005).

124   **2 Methodology**

125   **2.1 Field campaign 2019**

126   Based on required parameters (wave height, wave period, wave direction, bathymetry), the measurement campaign
127   in July 2019 was set up to assess the wave transfer from offshore (~25 km) to nearshore along two transects at the
128   western coast of the MD. The offshore measurement locations (OS1 and OS2), the measured bathymetry profiles
129   and the ERA5 grid are given in **Figure 2**. The offshore measurement points were thereby defined according to the
130   ERA5 grid cells closest to the coast, compring a resolution of 0.5° (approx. 55 km). The nearshore locations (NS1
131   and NS2) were chosen according to the water depth of a potential breakwater construction (1.5 – 2 m) with a
132   distance to the coastline of ~500 m for the northern (transect 1) and ~2.5 km for the southern profile (transect 2).
133   Each transect therefore could be allocated to a specific ERA5 gridbox, featuring a perpendicular alignment towards
134   the coastline. As shown in **Figure 2**, the position of OS1 was located some kilometres north to the perpendicular
135   line of transect 1 and NS1. Due to the parallel shape of the coastline bathymetry, and the deepwater conditions at
136   these locations which neglect the effect of the bottom friction to the wave height, OS1 was anyhow considered as
137   plausible input for transect 1 within this study.

138
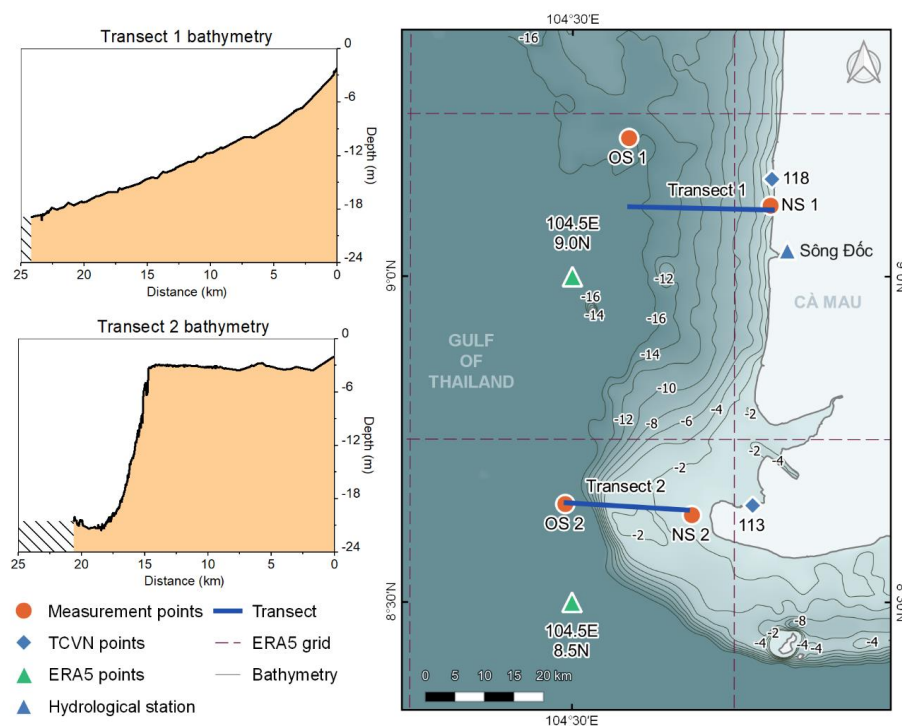
Figure 2: Western coast of the MD showing measurement locations (OS 1&2, NS 1&2) and bathymetry measured during the campaign in July 2019. ERA5 grid and national standard points (113 and 118 according to TCVN) along two transects (transect 1 and transect 2).

Onsite data were collected from 01st July 2019 to 13th July 2019. This time was chosen to capture the peak of the southwest monsoon season in the MD. Former campaigns often focused on the rather calm end of the monsoon season and performed mainly multiple short successiv single point measurements spread along the coast (Albers and Stolzenwald 2014; Marchesiello et al. 2017). Therefore, single measurements are difficult to compare and interpret. In contrast to former measurements, it was therefore intended to collect data especially from heavy sea states and over a period of several days simultaneously with several sensors.

Wave and current conditions along each transect were measured over a period of at least three days by ADCP (Acoustic Doppler Current Profiler) sensors, using a Signature 1000 (Nortek) for nearshore and AWAC (Acoustic Wave And Current Profiler; Nortek) for offshore measurements applying 10 min to 15 min measurement intervals. Data extraction and processing was later performed using the SignatureWaves64 software (Nortek). For comparison with the hourly wave heights and periods from ERA5, an average was calculated for the same timesteps from the measured data and later used for verification.

The bathymetry along each transect was measured by echo-sounding performed during the same period. As the boat could not approach the shallow water close to the coast at transect 2, the bathymetry for the last 3 km towards the coast could not be measured. The missing distance was completed using bathymetry data from a measurement in 2011, provided by the ICOE (ICOE 2012). For comparison especially within the 2D-model, the water levels were referenced to the water level measurements at Song Doc.

2.2 Long-term average and extreme conditions based on ERA5 reanalysis

Statistic analyses based on the latest, fifth-generation reanalysis of the European Centre for Medium-Range Weather Forecasts, ERA5 (Hersbach et al. 2020), serve as input to the SwanOne and Delft3D models. Integrated ocean wave parameters, and 10 m neutral wind speed and wind direction were downloaded from the C3S

163   (Copernicus Climate Change Service) Climate Data Store (Hersbach et al. 2018) at 0.5° spatial and hourly temporal
164   resolution. For the statistical description of average and extreme ocean wave conditions at the western coast of the
165   Ca Mau peninsula, significant wave height, maximum individual wave height, peak wave period, and mean wave
166   direction data are used for the 40-year period from 1979 to 2018. The same data for the year 2019 are used for the
167   comparison with the measurements taken during the field campaign in July 2019. Within all analyses, the two
168   ERA5 grid points centred at 9.0°N and 8.5°N at 104.5°E are used (Figure 2). These are the grid points closest to
169   the coast, both at a distance of approximately 25 km to the western coast of the Ca Mau peninsula. ERA5 was
170   chosen due to its high temporal resolution, which is particularly favourable for the investigation of extreme
171   conditions, and due to its long-term availability. This decision is based on a previously done comparison of ERA5
172   with WAVEWATCHIII (van der Linden et al. 2020). ERA5 exhibited an overall satisfactory performance when
173   compared with satellite-based data and in-situ measurements over the study region (see Sect. 3.1).

174   For the analysis of extreme conditions, return levels for 10-, 20-, 30-, 50-, and 100-year return periods were
175   estimated using a generalized extreme value distribution for wind and a Gumbel distribution for significant wave
176   height (cf. van den Brink and Können 2011). Maximum individual wave heights, and peak wave period were
177   analysed in the same way. To focus on wave and wind forcing that has a direct impact on the western coast of the
178   Ca Mau peninsula only, annual maxima, which are used as input to the estimation of return levels, are determined
179   only for timesteps with mean wave direction and 10 m neutral wind direction between 225° and 315°, respectively.
180   As an example, **Figure 3** shows the estimation of return levels of the maximum individual wave height (HMAX)
181   at transect 1. It should be noted that this precondition excludes, for example, waves associated with well known
182   Typhoon Linda in 1997 (Aschariyaphotha et al. 2011; Takagi et al. 2014; Takagi et al. 2015; Anh et al. 2019).

183   Another important input parameter to the 1D model, which is, however, not available from the ERA5 reanalysis,
184   is the water level. For the estimation of return periods of the water level, measurements from Song Doc (cf. **Figure**
185   **2** for the location of the station) are used. The longest available period of measurements from Song Doc was 1996–
186   2015. Return levels are estimated using a Gumbel distribution and are based on annual maxima during the rainy
187   season, i.e., May to October, and thus focusing on the season with predominantly southwesterly to westerly winds
188   and waves.

189   In addition to the extreme values based on the statistical analysis, a historical, long-lasting extreme event was
190   selected for a more detailed analysis. The selection of a single extreme event was based on three criteria, applied
191   to data of the two ERA5 grid points:

192   1. The mean wave direction is between 225° and 315°.
193   2. The 95th percentile of significant wave height (Hs) is reached or exceeded during at least 12 hours per day.
194   3. At least three consecutive days fulfil the first two criteria.

195   For long-lasting events, the last criterion was relaxed to allow up to two days in-between that did not fulfil the first
196   and/or second criterion. Based on these criteria, the eight-day period from 16th August until 23rd August 2000 was
197   selected. At the two ERA5 grid points the maxima of Hs were reached on 22nd August (2.41 m) and 21st August
198   2000 (2.59 m), corresponding to approximately 32- and 28-year return periods at transect 1 and transect 2,
199   respectively.
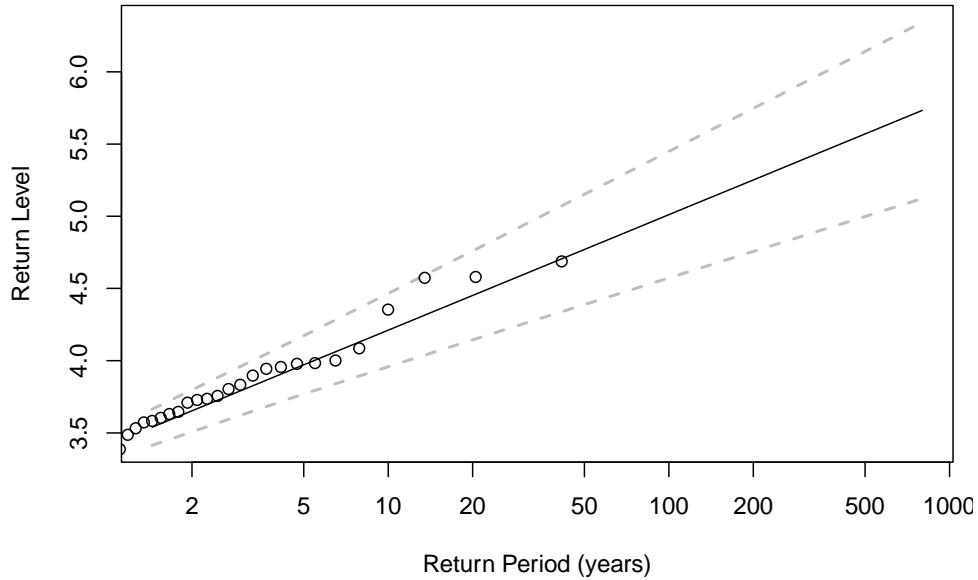
Figure 3: Example for the estimation of return levels. Return levels of HMAX (in m) for different return periods.

201

2.3 Numerical modelling

202

2.3.1 Model descriptions

203

Within this study SWAN was used to simulate the propagation of waves from offshore to nearshore comparing
1D and 2D model results. SwanOne transforms offshore wave conditions to nearshore using the 1D-mode of the
full SWAN package (The SWAN team 2018). SWAN (Booij et al. 1999) thereby utilizes Euler technique for time
discretization to solve the spectral action balance equation (3.1). Compared to other third-generation wave models
e.g. WAM or WaveWatch III, SWAN additionally considers triad wave-wave interactions and depth-induced wave
breaking.

204
205
206
207
208
209

$$\frac{\partial}{\partial t}N + \frac{\partial}{\partial x}c_x N + \frac{\partial}{\partial y}c_y N + \frac{\partial}{\partial \sigma}c_\sigma N + \frac{\partial}{\partial \theta}c_\theta N = \frac{S}{\sigma} \qquad (3.1)$$

210

On the left hand side of (3.1) the wave action density $N(\sigma,\theta)$ is used instead of energy density ($N=E/\sigma$). c_x, c_y are
propagation velocities in geographical space, while c_σ and c_θ are propagation in spectral space σ and θ.

211
212

The source term on the right-hand side of (3.1) according to (Hoque et al. 2020) consists of:

213

$$S = S_{in} + S_{wc} + S_{nl4} + S_{bf} + S_{nl3} + S_{br} \qquad (3.2)$$

214

in which S_{in} is wind-generated waves; S_{wc} is dissipation due to whitecapping; S_{nl4} is nonlinear quadruplet wave-
wave interaction; S_{bf} is dissipation due to bottom friction; S_{nl3} is nonlinear triad wave-wave interaction; and S_{br} is
depth-induced wave breaking. While the first three sources are important in deep water, the later three are
significant in shallow water.

215
216
217
218

Within this study, the 1D (SwanOne) and 2D (Delft3D-WAVE, furtheron refered to as Delft3D) applications of
SWAN are used to simulate the same scenarios and later compare their results during validation with in-situ data.
SwanOne thereby uses the above 2D descriptions but neglects one dimension of the geographical space.
Additionally, the simulation is only calculated in a stationary mode. This is reasonable for applications for small
areas, where bathymetry contour lines stay relatively parallel to each other and the coast, and stationarity
assumptions of instantaneously reacting waves to the wind field fluctuation are acceptable (Rogers et al. 2007).

219
220
221
222
223
224

225   The 1D-mode assumes that the offshore bathymetry can be represented by parallel bottom contours such that the
226   bottom profile can be specified along one transect normal to the average coastline. The SWAN model represents
227   the wave field in terms of the 2D-frequency-direction wave spectrum which then evolves towards the coast
228   including effects of wind, current, water level, depth, shoaling and refraction effects.

229   The 2D wave application is coupled with the numerical hydraulic module, Delft3D-FLOW. Delft3D-FLOW
230   utilizes finite difference methods to solve the Navier-Stokes equations under shallow water assumption. The
231   computational grid thereby can be rectilinear or curvilinear. Nesting techniques are available to combine different
232   grid sizes and grid formations (H. Gerritsen et al. 2008).

233   Each module is responsible for specific hydrodynamic processes. However, they can be coupled in integrated
234   simulations for complex simulations when necessary. Within this study, the Delft3D version 4.04.01 was used.
235   The aim was to describe the dominating main physical processes of interest which consisted of tidal regime,
236   nearshore wind wave development, tidal-induced current, and wave-induce current.

2.3.2 Model setup and verification approach

238   The offshore measured wave heights, periods and directions together with ERA5 wind parameters were used as
239   input to SwanOne. Data at OS1 and OS2 where applied at the offshore boundary of the bathymetry profile. The
240   waves are then transferred towards the coast where they were extracted again at the locations of the nearshore
241   sensors for both transects. A sketch of the input parametes and their representation in SwanOne is given in the
242   supplementary materials (SM1). The bathymetries along each transect were implemented according to the
243   measured data (see **Figure 2**). All data were adapted to local time (UTC + 7 h) and are given in UTC afterwards.
244   Wind speed and direction were taken from ERA5 for both steps due to lacking in-situ data. According to the
245   availability of ERA5 wind and wave data with a 1h resolution, the modelling was performed for 1h timesteps,
246   therefore comprising averages of the measured sub-hourly values wave height and period. For SwanOne, each
247   timestep needed to be individually calculated, with separate data input. Wave heights thereby where implemented
248   as single wave heights. Wave spectrum would be possible as well, however wave heights were used within this
249   study. Bottom friction could not be included based on the restriction of the software. Input of currents would have
250   been possible, however the single point current measurements showed unconfident values and were therefore
251   discarded.
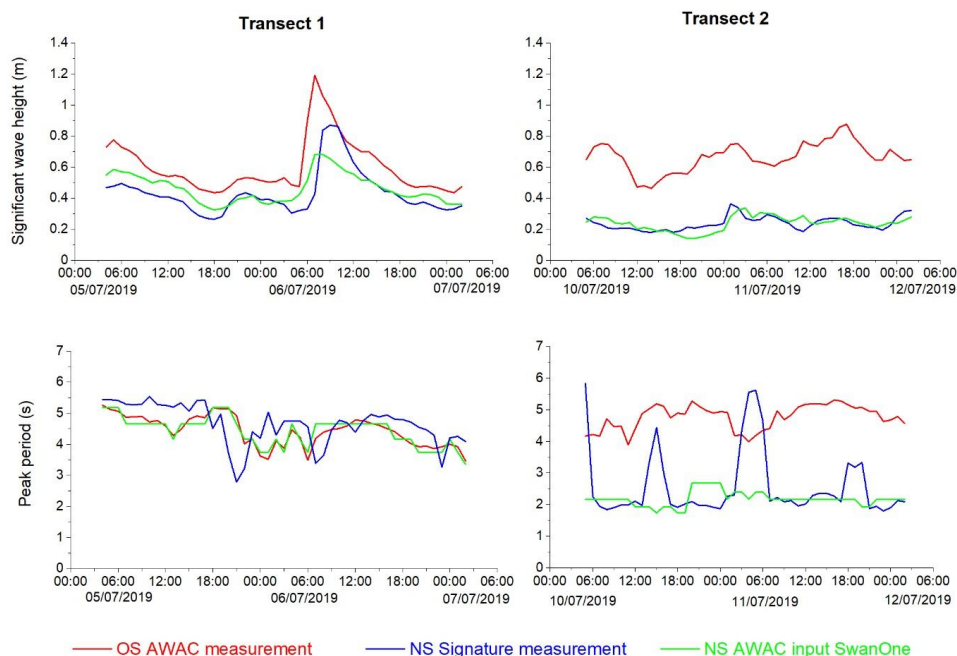
Figure 4: Comparison of AWAC measurement, Signature 1000 measurement, Wave transfer of AWAC measurement with SWAN to signature location (Within the publication, the wave period from here on is referring to the wave peak period).

Within the verification process (see Figure 4), the measured offshore wave heights (AWAC, red line) where transferred towards the nearshore and extracted again at the location of the Signature 1000 sensor (green line), where they were compared to the measured wave heights (blue line). Apart from three pronounced peaks in the wave preiods at transect 2, which most likely originate from a sensor malfunction, the data for wave height and period shows good agreement for both transects to accept the applicability of the 1D transfer model for further use within this study. By using input data with resolution of 1 h (red), even a short-lasting storm event which happened during the measurement at transect 1 (start: 6th July 2019 5:00 UTC) could be reproduced successfully. The temporal shift between measured and transferred waves at the beginning of the storm might be attributed to the northern position of the AWAC sensor as described in **Fehler! Verweisquelle konnte nicht gefunden werden.**.

For the 2D-model, the bathymetry boundary is a combination of Gebco_2020 grid for the offshore area (GEBCO Bathymetric Compilation Group 2020), while the nearshore zone, especially the area of interest, was supplemented with nearshore measurements from three field investigation campaigns. Two campaigns were carried out by ICOE in 2011 (ICOE 2012) and 2016 (ICOE 2017), where the first focusing on Ca Mau cape topography while the later investigated the northern part of the western coast with 15 cross profiles. In 2019, the already mentioned campaign by KIT and SIWRR investigated three more cross profiles with a length of 20 km - 25 km towards the coast.

Wind force was implemented by applying hourly ERA5 data of 10 m wind field for the whole domain (Hersbach et al. 2018). Wave boundaries were regulated by hourly ERA5 data of wave conditions. Delft3D-WAVE was coupled with Delft3D-FLOW for fully simulating wave-current interaction within the surf zone. Tidal fluctuations were interpreted from TPXO 8.0 tidal constituents for Delft3D-FLOW (Egbert and Erofeeva 2002).

9

275
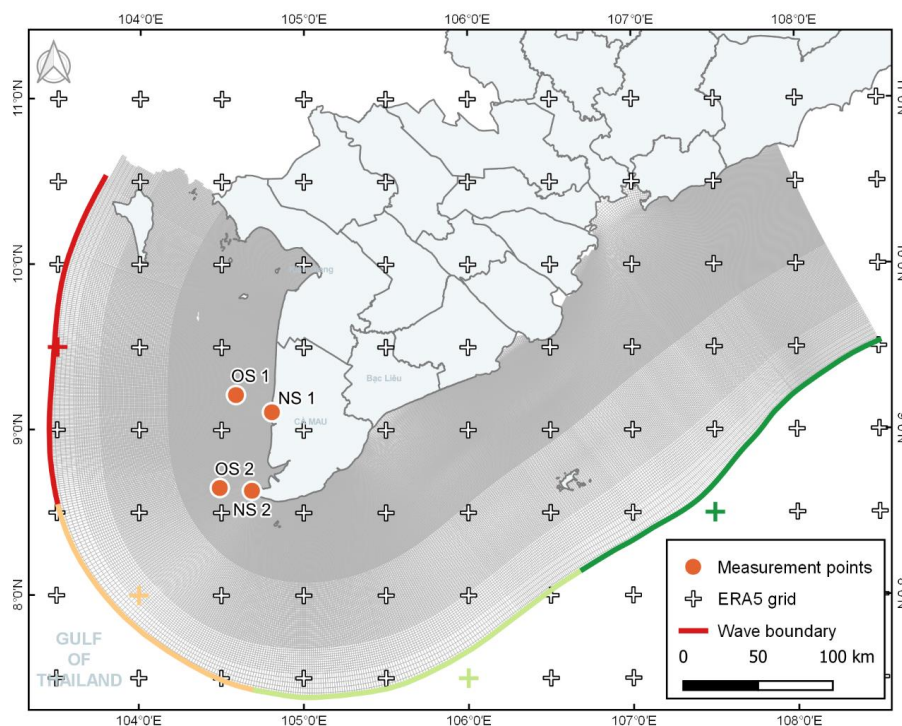
Figure 5: Grid of the 2D model including the four different sections of boundary conditions (wave and wind input, referring to ERA5 grid) and the sensor locations.

278   A loop of adjustment and calibration for the 2D model was performed stepwise for the domain extent, grid type
279   and grid resolution (see supplementary materials SM2, SM3, SM4, SM5, SM6), and the wave and wind boundary
280   definition. The optimization process aims to achieve good agreement between simulation and measurement data
281   while maintaining reasonable computational time. Along the process it was found that grid resolution has a stronger
282   impact on accuracy than grid type (rectangular or curvilinear). However, curvilinear, in this case, gives the
283   flexibility to optimize the grid resolution in the nearshore area. A map of the final curvilinear grid, the boundaries
284   and the referring ERA5 wind and wave locations are given in **Figure 5**. Besides, the swell appeared to have a
285   substantial impact on the results as well, therefore, applying wave conditions at offshore boundary gives higher
286   efficiency in improving the swell wave prediction, in comparison to an extention of the simulation domain. Despite
287   it was recommended to use $0.019 \ m^2 \ s^{-3}$ for JONSWAP bottom friction in the condition of a smooth seafloor (The
288   SWAN team 2018) the default value of $0.067 \ m^2 \ s^{-3}$ showed better agreement, especially when verifying with
289   nearshore measurements. The overall process of optimizing the model accuracy is illustrated in the supplementary
290   materials (SM7).

291   **3. Results and Discussion**

292   **3.1 Model verification**

293   In a second step, the same approach (Sect. 2.3.2.) was done with wave heights taken from ERA5 over the same
294   period as the onsite measurements. For comparison, all modelling results (1D and 2D) were illustrated together
295   with the offshore and onshore wave heights and wave periods measured during the field campaign (see **Figure 6**).
296   The overall range of the measured offshore wave heights and the wave heights taken from ERA5 show a good
297   agreement for transect 1 until the 6th of July 2019 at 6:00 UTC and for transect 2 over the entire period. This agrees
298   as well to the offshore conditions in the 2D-model. The values for transect 1 after this date show a strong increase
299   of the measured wave heights due to a sudden local storm event that lasted for approx. 10 hours but was not

300   reproduced in the ERA 5 data (dashed blue line). It becomes obvious, that such short and locally confined events
301   are not sufficiently replicated by the coarse grid cells of ERA5 in comparison to the single point data measured by
302   the sensors. While wind speeds of ERA5 showed highest values within this period with 9.6 and 9.9 m s^{-1} at transect
303   1 and transect 2, respectively, the storm did not last long enough to generate comparable wave heights by wind
304   fetch within the 2D-model (dashed green line) in comparison to the measured wave heights (dashed red line). Due
305   to these reduced input wave heights, the nearshore output of the 2D-model features this peak as well with much
306   lower wave heights. As both models are based on the same ERA5 input regarding wave height, wave periods and
307   wind speed and directions, this could be attributed to the stationary mode of the 2D-model, where each timestep
308   is influenced by the results of the timestep before and therefore wind effects might constantly influence the model
309   while the boundary wave heights remain small (dashed blue line).

310   Wave periods were also compared between measured data (AWAC and Signature 1000 sensors) and the simulation
311   results (Delft3D and SwanOne; see **Figure 6**). At transect 1, the wave peak periods both offshore and nearshore
312   overall vary between 3 and 5.5 seconds without a pronounced reduction during the transfer from offshore to
313   nearshore. For data featuring the same origin, like AWAC and Signature 1000 (solid and dashed red line) or like
314   ERA5 input and SwanOne (solid and dashed blue line) the peak period rather remains constant from offshore to
315   nearshore. This might be an effect of the shallow but continuously increasing bathymetry (see **Figure 2**) where
316   the waves spectrum is not converted along its way and therefore are not breaking.

317   In contrast, transect 2 shows a clear reduction of peak periods from offshore to nearshore for measured and
318   modelled data. Wave periods vary from 4 to 5.2 seconds in the offshore and reduce to 1.8 to 2.2 seconds at the
319   nearshore. This is as well an effect of the bathymetry (see **Figure 2**), where the sudden seafloor increase at the
320   edge of the shelf is converting the wave towards a smaller peak period. Despite the three already mentioned peaks
321   in the wave period, the SwanOne results (blue solid line) agree well with measured data (red solid line), while the
322   Delft3D results (solid green line) provided slightly lower wave periods (1.8 to 2 seconds). The difference of wave
323   periods between measurements and numerical results are approx. 20% at both transects (ignoring the peaks) at the
324   offshore and nearshore locations.

325   Beside the described lack of accuracy for short extreme events, both numerical platforms showed sufficient
326   agreement, especially at transect 2, so the overall applicability for the further investigation was considered reliable.
327   As mentioned in Sect. 2.3.1, the 1D-model is operated only in a stationary mode, so each single run is only based
328   on its single timestep input. Subsequently, the 1D-model transfers this data to the nearshore. To increase the 1D
329   model reliability as well over longer periods, both models were compared in the following over a several days
330   lasting storm event.
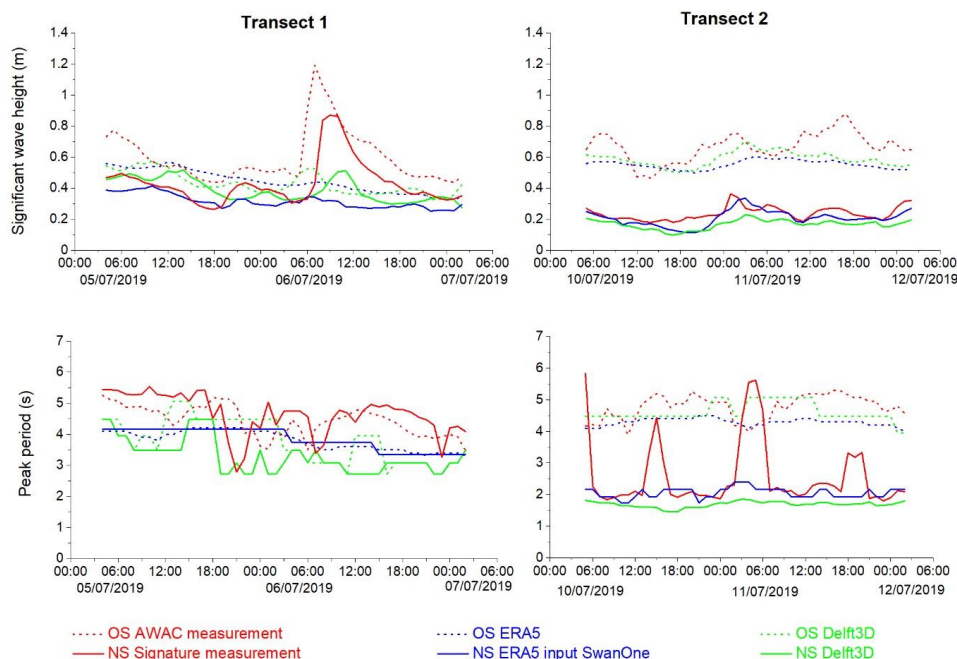
Figure 6: Wave heights and wave period at transect 1 and transect 2, taken from measurements, ERA5 reanalysis, as well as from SwanOne and Delft3D models.

3.2 Applications

3.2.1 Long-lasting extreme event

Before focusing on mean and extreme ocean wave conditions based on a statistical analysis of ERA5 data in the next section, a quantitative comparison of results when applying 1D and 2D approaches to a historical, long-lasting extreme event in August 2000 is provided here. Since no long-term, in-situ measurements are available for the study region, ERA5 data was used for the selection of the event. The criteria for the selection of the historical extreme event are described in section 0. The long-lasting extreme wave conditions between 16th and 23rd of August 2000 were related to enhanced westerly low-level winds. One factor favouring an enhanced monsoon flow was tropical storm Kaemi. According to best track data of IBTrACS (International Best Track Archive for Climate Stewardship; Knapp et al. 2010; Knapp et al. 2018) Kaemi formed on 18th August 2000 over the South China Sea and made landfall in central Vietnam on 22nd August 2000. In addition, the convectively active phase of the Madden–Julian Oscillation (MJO; Madden and Julian 1972) was located over the Maritime Continent at that time as indicated by the real-time multivariate MJO index (Wheeler and Hendon 2004). Since the convectively active phase of the MJO can lead to enhanced westerly winds during the rainy season over southern Vietnam (van der Linden et al. 2016) this might be another factor that contributed to the extreme wave conditions. According to the ERA5 reanalysis the highest significant wave heights during the event, reaching more than 2.5 m, occurred on 22nd and 21st of August at the offshore locations of transects 1 and 2, respectively (blue dashed lines in **Figure 7** top left and top right).

Figure 7 shows the comparison of Hs (top) and Tp (bottom) between ERA5 and Delft3D at the offshore locations (blue and green dashed lines) and SwanOne and Delft3D at the nearshore locations (blue symbols and green solid lines) of both transects. The output timesteps of Delft3D and ERA5 are hourly, while a 6-hourly output from SwanOne was used, which could lead to a misrepresentation of local minima or maxima. For the interpretation of the results it should also be noted that ERA5 served as input for both SwanOne and Delft3D, due to the non-availability of in-situ measurements.

12

358 The agreement between Hs from ERA5 and Delft3D is overall good at the offshore locations of both transects
359 (**Figure 7** top, dashed green and blue lines). The agreement does not depend on the wave heights and small
360 deviations of Delft3D with respect to ERA5 (biases not larger than ±20%, e.g. between 18th and 20rd August 2000
361 at transect 2) seem not to be systematic. The overall good agreement does not come fully unexpected due to the
362 calibration of Delft3D against ERA5 (see SM7) and due to the use of 10 m neutral winds from ERA5 over the
363 entire domain (compare **Figure 5**). However, since ERA5 wave spectra were only used as input at the outer
364 boundaries of the model domain (**Figure 5**), this demonstrates that the calibration of Delft3D worked well. When
365 focusing on the nearshore locations, SwanOne and Delft3D show a good agreement at transect 1 (**Figure 7**, top
366 left). At transect 2 (**Figure 7**, top right), Hs is almost constant over the entire period at the nearshore location,
367 leading to larger differences to SwanOne, which shows more pronounced fluctuations that correspond to the ERA5
368 input at the offshore location. Possible explanations of the differences of Hs are the very shallow bathymetry at
369 transect 2 and differences between the bathymetries used in SwanOne and Delft3D (see supplementary materials,
370 SM8). In SwanOne, higher waves and more pronounced fluctuations at the nearshore location are possible due to
371 higher water levels.

372 When focusing on the same comparisons for Tp (**Figure 7**, bottom row), larger differences can be observed
373 between the two transects. At transect 1, almost no decrease of the Tp between the offshore and nearshore location
374 occurs (**Figure 7**, bottom left). At both locations, Tp varies between approximately 4 and 7 seconds. Overall, Tp
375 is up to approximately 1 second shorter in Delft3D. At transect 2, however, Tp at the nearshore location is only
376 half of Tp at the offshore location, decreasing from approximately 6 seconds to 3 seconds (**Figure 7**, bottom right).
377 The offset of Delft3D compared to ERA5 and SwanOne is comparable to that at transect 1. As could be seen for
378 Hs at the nearshore location, the temporal variation of Tp at the nearshore location is very weak in Delft3D when
379 compared to SwanOne. The differences in Hs as well replicate the results from the measurement campaign (see
380 **Figure 6**) and are therefore most likely caused by the same bathymetry effects.
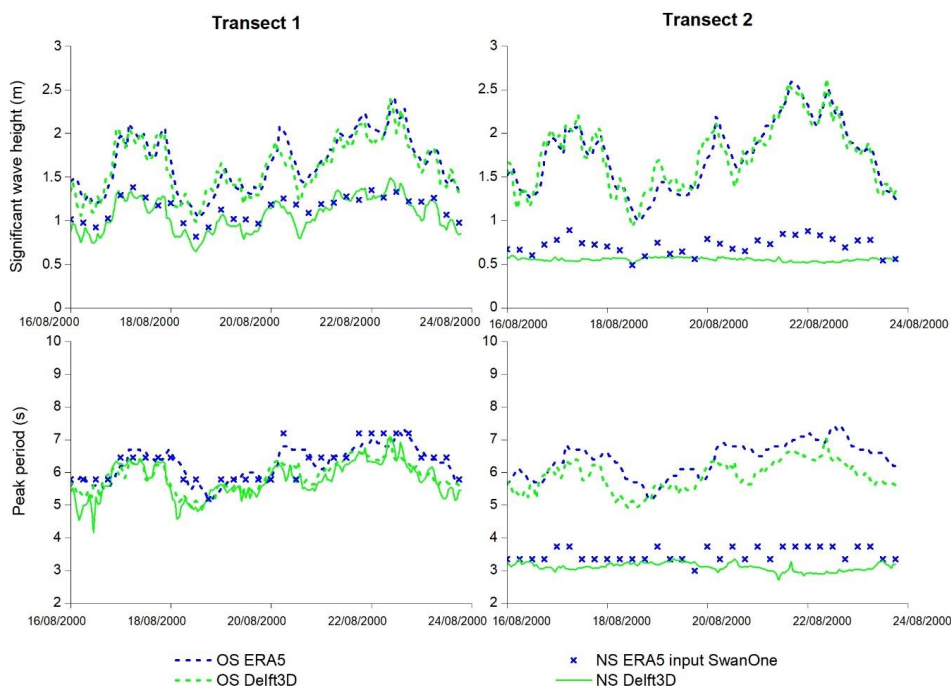

381

382 **Figure 7: Wave transferring from offshore to the coast at transect 1 and transect 2 in 2000**

383 In addition to the different bathymetries used in the two modelling approaches that could lead to differences in Hs
384 and Tp, as discussed above, there are various other potential reasons. Particularly, it is expected that Delft3D could
385 better represent the wave conditions since it considers important factors such as wind surge, wave diffraction,

386 wave–wave interactions and wave–current interactions. All of these factors are not considered in SwanOne. Swell,
387 which was found to be essential in the correct simulation with Delft3D (cf. Sect. 2.4), is considered in both models
388 through the use of ERA5 input. Despite the uncertainties due to the bathymetries being used in this shallow coastal
389 area, **Figure 8** illustrates the advantages of the 2D approach, where Hs and Tp at one timestep during the first
390 period of enhanced wave heights (00:00 UTC on 17th August 2000) are shown as an example. Using Delft3D,
391 wave conditions can easily be derived for any other location along the coast, therefore result extraction only
392 depends on the grid resolution of the model. Simulating ocean waves over a larger domain also allows for
393 interaction not only with other waves, currents, and the atmosphere but also with topographic features, which
394 manifests, e.g., in wave attenuation and diffraction at islands in the Gulf of Thailand. On the contrary, SwanOne
395 only considers a simple, one-way interaction with the atmosphere and strongly depends on the grid spacing of the
396 input wave conditions. One major advantage of SwanOne thereby is its applicability to wave conditions derived
397 from statistical extreme value analysis.
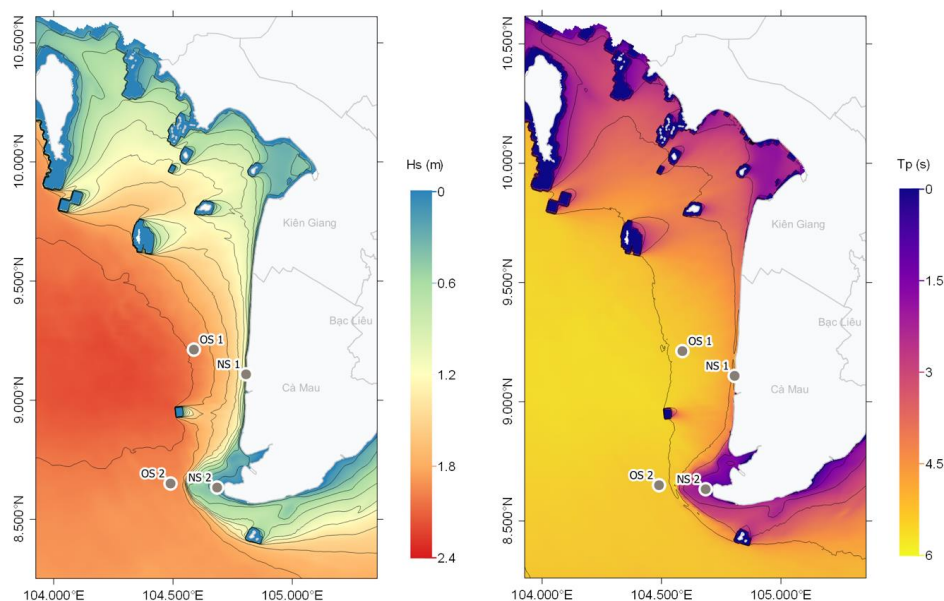
398 **Figure 8: Extreme period of oceanographic condition at 00:00 UTC on 17th August 2000) (left: wave height (m), right:**
399 **Wave period (s)).**

400 **3.2.2 Average and extreme conditions for different return periods**

401 According to local dyke regulations, the coastal protection for the MD needs to consider a return period of 20 to
402 30 years, based on the agricultural use and the population density of the protected hinterland (MARD, 2012).
403 However, within this study, the calculations were additionally done for longer return periods of 50 and 100 years
404 (see **Table 1**).

405 **Table 1: Input parameters for the 1D wave transfer model along transects T1 and T2.**

Transect	Variable	Mean	Return period [years]				
			10	20	30	50	100
T1	Wind speed [m s⁻¹]	5.80	12.88	13.38	13.68	14.07	14.62
	Hs [m]	0.68	2.19	2.32	2.40	2.49	2.62
	HMAX [m]	1.28	4.18	4.42	4.57	4.74	4.98
	Wave period [s]	4.34	7.39	7.66	7.81	8.00	8.26
T2	Wind speed [m s⁻¹]	6.02	13.28	13.80	14.10	14.47	14.98
	Hs [m]	0.75	2.36	2.51	2.61	2.72	2.87
	HMAX [m]	1.41	4.51	4.81	4.99	5.20	5.49

	Wave period [s]	4.61	7.50	7.76	7.91	8.10	8.36
All	Water level variation [cm]*	–	96.15	104.84	109.84	116.10	124.53

406   *water level refers to Song Doc (see **Figure 2**)

407   The input parameters for the wave transfer calculation are given in Table 1. The wave and wind parameters were
408   extracted and analysed based on the ERA5 data from 1979 to 2019. As described in Sect. 2.2, only waves from a
409   western direction were considered within this evaluation, therefore comprising mostly waves during the southwest
410   monsoon season. The water level variations for the different return periods are based on measurements of the Song
411   Doc hydrological station (see Figure 2) from 1996 to 2019 following the same statistical evaluation as done for
412   the wave height (see Sect. 2.2). Due to the lack of long-term local sea level data, average water levels at Song Doc
413   were applied for both transects following the assumption that there is not much variance of water level along the
414   western coast. Water level variations in Table 1 therefore comprise a combination of wind surge and tides.

415   Results for Hs are presented in Figure 9 for return periods of 10 years (green), 20 years (blue) and 50 years (red).
416   The left column shows the decrease in wave height while the wave is transferred from offshore (25 km) to
417   nearshore (1 km), the right column gives a focus on the last 1000 m towards the coast. As expected, for the
418   intermediate and shallow water conditions, the wave height mainly follows the bathymetry profile, featuring a
419   slight, constant decrease along the slowly rising bathymetry of transect 1 and a sudden change at approx. 15 km
420   distance to coast, where the shelf plateau drops steeply for transect 2.
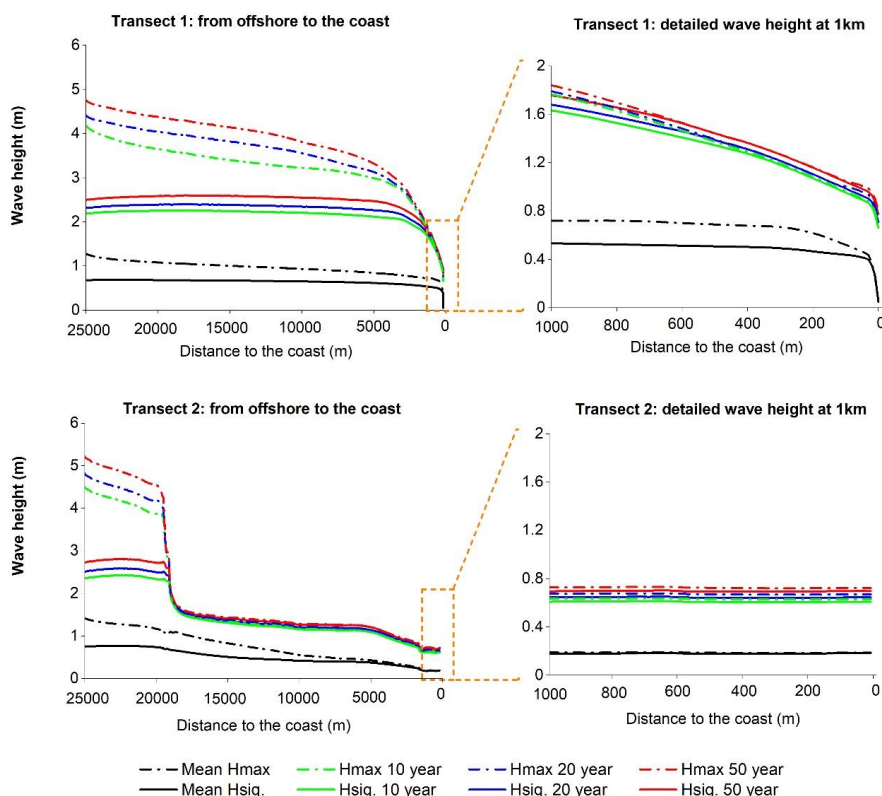
421

422   **Figure 9: Design condition results for T1 and T2 calculated with SwanOne based on the input of Table 1.**

423   The long-term average wave heights along the last km, apart from the final 100 m, ranges around 0.5 m at transect
424   1 and 0.2 m at transect 2. Maximum average wave heights at transect 1 are around 0.7 m while and are therefore
425   substantially higher than the maximum average wave heights at transect 2.

15

426 These numbers are in good agreement to average nearshore significant wave heights from previous surveys with
427 0.5 m up to 0.85 m at the western coast of the MD (Nguyen et al. 2020). Results at Soc Trang for wave
428 transformation from offshore to nearshore using the XBeach model show as well comparable results reducing a
429 2 m wave at 10 km down to 0.5 m at the beach for comparable bathymetry conditions like transect 1 (Phan et al.
430 2015).

431 Related to the coastal protection, e.g. by detached breakwaters, wave heights for return periods of 20 years in a
432 realistic implementation distance between 100 m up to 300 m to the coast ranging from 1.1 m to 1.3 m at transect
433 1 and 0.65 m at transect 2 (compare **Figure 9**). Maximum wave heights for the same return period and distance
434 show negligibly higher values for both transects. This might be attributed to the fact, that the wave heights in
435 shallow water near to the coast are already close to the physical limit.

436 Tas (2016) followed a similar approach as presented in this study, calculating the wave transfer with SwanOne
437 and SWASH for wave height conditions which were calculated based on NOAA wind data over a fetch over
438 250 km assuming a water depth of 65 m. The model was applied as well over the last 25 km towards the coast.
439 However, as to our own measurements the water depth is only approximately 20 m at this distance, the input wave
440 height of up to 8 m are most likely overestimating the real conditions.

441 As a well known fact, wave heights are significantly dependent on the water depth especially for the shallow
442 nearshore zone. Increasing water levels therefore would directly increase the maximum possible wave height at
443 the coast. Under extreme weather conditions, water levels could as well rise due to stable wind stress (wind surge).
444 This phenomenon was demonstrated using Delft3D by coupling the two modules Wave and Flow and applying
445 winds with constant high speeds and direction to the model over an extended period of time (see SM9). Within
446 this test, the water depths are increased for approx. 1 m at a constant wind scale of 9 while they are up to 2 m at a
447 wind scale of 11, therefore demonstrating a kind of worst case wind swell scenario. However it must be emphasized
448 that increasing water depths on the one hand allow for higher waves but as well increase the submergence of any
449 breakwater and the overtopping of waves. Therefore, extreme surge conditions would not inevitably lead to a
450 adaption of the breakwater design regarding its stability, as the whole breakwater is most likely submerged. Under
451 such conditions the waves can again hit the coastline without any prior reduction.

452 **3.3 Limitations of the study**

453 According to the different input sources, wave heights were available as Hs (calculation based on measured wave
454 heights) and Hm0 (statistical analysis based on energy spectrum) from the sensors, while ERA5 only features
455 Hm0. To remain consistent, all calculations were done based on Hm0. As a comparison of Hs and Hm0 for the
456 measurements showed slightly higher values for Hm0 (around 5%), these results therefore might overestimate the
457 significant wave height.

458 While the AWAC at transect 1 showed reasonable data regarding the wave directions, the wave directions at T2
459 where rather inconsistent. During launching the wave sensor in the field, the AWAC sensor at transect 2 was tilted
460 by around 12°, which is slightly above the suggested operation range (10° according to Nortek). Nevertheless, it
461 was still below the acceptable limit of 20°. Therefore, tilt effects were removed during the post-processing of the
462 data. In addition, some of the measured wave frequencies were close to the range the sensors cut off which might
463 be an additional source for inaccuracies.The wind direction from ERA5 was taken as input for the wave direction
464 instead at transect 2 as both typically coincide if the wind comes from a constant direction over longer periods.

465 As mentioned above, it must be noted that the measured data quality at transect 2 was rather inconsistent, hence
466 results at this transect should be treated with caution. However, due to the fact of high agreement between the 1D
467 and 2D numerical approaches, the selection of alternative boundary conditions in case of inadequate sensor
468 measurements seems sufficient. Therefore, we decided to present these results within this study, as the availability
469 of data and related studies is scarce within this area. Besides, transect 2 for practical reasons is of minor relevance,
470 as it is located at the tip of the Ca Mau peninsula, an area of natural soil deposition process, with no need for
471 coastal protection.

16

4 Conclusions

Within the presented study, a stepwise approach for the determination of dimensioning conditions for breakwater design is presented based on a combination of measurements, long-term reanalysis data and numerical approaches. Within the first step, measured data and ERA5 offshore data could be successfully transferred to onshore locations with SwanOne and Delft3D, where they could be verified by onshore measurements. Within a several days lasting storm event, both numerical platforms were used to demonstrate the applicability of the wave transfer approach based on ERA5 reanalysis data as input in the Gulf of Thailand. Both stepos thereby showe consistent results. Afterwards, SwanOne was used to calculate nearshore wave heights and periods for mean, 10-, 20-, 50- and 100-year return periods at the western coast of the MD, based on 40-year ERA5 data. Average wave heights here are in good accordance to previously published data. These results will further be used as dimensioning conditions within the design process of a breakwater to counteract the ongoing coastal erosion in the study area.

Within the comparison, both numerical approaches underestimate the extreme conditions compared to the measured values as a result of insufficient representation of the storm by ERA5 due to spatio-temporal resolution. Local measured wind data with high temporal resolution might increase the accuracy of the results, as it was intentionally planned but could not be considered due to technical problems during the measurement campaign.However, a offshore storm does not necessarily have to pass the station as well or with the same intensity.

Based on the investigations within this study, the models offer the following advantages and disadvantages:

SwanOne:

- The model is easily accessible and fast in simulation.
- Input data is only needed for the investigated site, so the calculation is possible based on a few single point measurements. However the results of this 1D approach are as well only limited along the investigated transect.
- Statistical numbers like wave heights and periods taken from return period analysis can easily be applied within this model.
- Some factors like bottom friction or the wind surge are not implemented within the simulation software. The results therefore might have some inaccuracies.

    Delft3D:

- Based on the spatial model setup, it is possible to extract simulation results at any location within the model domain.
- Wave-current interaction is considered to complete the picture of hydrodynamics in the nearshore zone. Compared to SwanOne where the current needs to be defined as input parameter, Delft3D is calculating them based on the other input parameters like wind speed and wind direction. The feature of continuous wind input (e.g. storm surge effects) and bottom friction are included and lead to a higher accuracy of the results as well.
- Due to its 2-dimensional character, a broad amount of input parameters (e.g. bathymetry, wind speed and directions) is required to set up the model.
- Besides, only real events in terms of subsequent temporal data series make sense to serve as input. Input data for variable return periods is therefore difficult to generate on a spatial level as spatial input data e.g. for a 100-year return period could not be generated from statistics.
- Due to its complexity, the whole model generation, the definition of boundary conditions and calibration process is time consuming.

As both numerical approaches proof their suitability to calculate nearshore wave heights and periods based on offshore reanalysis data, the simulation results in general can be recommended for determination of breakwater design conditions. However, a certain data quality and temporal resolution should be available.

17

Data availability

All raw data can be provided by the corresponding authors upon request.

Author contribution

MZ, RVDL, TCD, DHTV and NMN designed the sampling campaign and conducted the measurements. MZ, TCD, HTDV and NMN evaluated the measured data. TCD and HTDV performed the wave transfer modelling, RVDL prepared the ERA5 reanalyse data, MZ prepared the original draft with contributions of MZ, RVDL, TCD and DHTV. FS, PO, AHF and FN contributed in supervision of the research activities as well as in reviewing and editing.

Competing interests

The authors declare that they have no conflict of interest.

References

Albers, T.; San, Dinh Cong; Schmitt, K. (2013): Coastal Protection in the Lower Mekong Delta. Shoreline Management Guidelines. Available online at http://coastal-protection-mekongdelta.com, checked on 10/26/2021.

Albers, T.; Schmitt, K. (2015): Dyke design, floodplain restoration and mangrove co-management as parts of an area coastal protection strategy for the mud coasts of the Mekong Delta, Vietnam. In *Wetlands Ecology and Management* 23 (6), pp. 991–1004. DOI: 10.1007/s11273-015-9441-3.

Albers, Thorsten; Stolzenwald, Jan (2014): Coastal Engineering Consultancy in Ca Mau Province. Edited by GIZ - Deutsche Gesellschaft für Internationale Zusammenarbeit. Bonn and Eschborn, Germany.

Allison, Mead; Nittrouer, Charles; Ogston, Andrea; Mullarney, Julia; Nguyen, Thanh (2017): Sedimentation and Survival of the Mekong Delta: A Case Study of Decreased Sediment Supply and Accelerating Rates of Relative Sea Level Rise. In *Oceanography* 30 (3), pp. 98–109. DOI: 10.5670/oceanog.2017.318.

Anh, Le Tuan; Takagi, Hiroshi; Thao, Nguyen Danh (2019): STORM SURGE AND HIGH WAVES DUE TO 1997 TYPHOON LINDA: UNINVESTIGATED WORST STORM EVENT IN SOUTHERN VIETNAM. In *Journal of Japan Society of Civil Engineers, Ser. B3 (Ocean Engineering)* 75 (2), I_73-I_78. DOI: 10.2208/jscejoe.75.I_73.

Aschariyaphotha, N.; Wongwises, P.; Humphries, U. W.; Wongwises, S. (2011): Study of storm surge due to Typhoon Linda (1997) in the Gulf of Thailand using a three dimensional ocean model. In *Applied Mathematics and Computation* 217 (21), pp. 8640–8654. DOI: 10.1016/j.amc.2011.03.105.

Besset, Manon; Gratiot, Nicolas; Anthony, Edward J.; Bouchette, Frédéric; Goichot, Marc; Marchesiello, Patrick (2019): Mangroves and shoreline erosion in the Mekong River delta, Viet Nam. In *Estuarine, Coastal and Shelf Science* 226, p. 106263. DOI: 10.1016/j.ecss.2019.106263.

Booij, N.; Ris, R. C.; Holthuijsen, L. H. (1999): A third-generation wave model for coastal regions: 1. Model description and validation. In *J. Geophys. Res.* 104 (C4), pp. 7649–7666. DOI: 10.1029/98JC02622.

Chu Van Cuong; Sharon Brown; Huynh Huu To; Marc Hockings (2015): Using Melaleuca fences as soft coastal engineering for mangrove restoration in Kien Giang, Vietnam. In *Ecological Engineering* 81, pp. 256–265. DOI: 10.1016/j.ecoleng.2015.04.031.

Dao, Hoang Tung; Hofland, Bas; Suzuki, Tomohiro; Stive, Marcel J. F.; Mai, Tri; Le Tuan, Xuan (2021): Numerical and small-scale physical modelling of wave transmission by wooden fences. Journal of Coastal and Hydraulic Structures, Vol. 1 (2021): Single articles. DOI: 10.48438/JCHS.2021.0004.

Dastgheib, Ali; Reyns, Johan; Thammasittirong, Supot; Weesakul, Sutat; Thatcher, Marcus; Ranasinghe, Roshanka (2016): Variations in the Wave Climate and Sediment Transport Due to Climate Change along the Coast of Vietnam. In *JMSE* 4 (4), p. 86. DOI: 10.3390/jmse4040086.

Duy Vinh, Vu; Ouillon, Sylvain; van Thao, Nguyen; Ngoc Tien, Nguyen (2016): Numerical Simulations of Suspended Sediment Dynamics Due to Seasonal Forcing in the Mekong Coastal Area. In *Water* 8 (6), p. 255. DOI: 10.3390/w8060255.

Egbert, Gary D.; Erofeeva, Svetlana Y. (2002): Efficient Inverse Modeling of Barotropic Ocean Tides. In *Journal of Atmospheric and Oceanic Technology* 19 (2), pp. 183–204. DOI: 10.1175/1520-0426(2002)019<0183:EIMOBO>2.0.CO;2.

Franca, M. J.; Juez, C.; Kurniawan, A.; Zemann, M. (2022): Case Studies of Sediment Mining Activity∗. In : Reference Module in Earth Systems and Environmental Sciences: Elsevier. Available online at https://www.sciencedirect.com/science/article/pii/B9780128191668001948.

GEBCO Bathymetric Compilation Group (2020): The GEBCO_2020 Grid - a continuous terrain model of the global oceans and land.

Groenewold, S.; Peters, S. (2016): Integrated Coastal Protection And Mangrove Belt Rehabilitation In The Mekong Delta. Pre-feasibility study for investments in coastal protection along 480 kilometers. With assistance of Dr. Nguyen Nghia Hung, Dr. Lam Dang Thanh, Dr. Thinh Pham Trong, Dr. Ho Dac Thai Hoang, Dr. Dinh Cong San. Edited by GIZ - Deutsche Gesellschaft für Internationale Zusammenarbeit. Bonn and Eschborn.

H. Gerritsen; E.D.de Goede; F.W. Platzek; J.A.Th.M. van Kester; M. Genseberger; R.E. Uittenbogaard (2008): Validation Document Delft3D-FLOW. A software system for 3D flow simulations. Deltares. Available online at https://oss.deltares.nl/c/document_library/get_file?uuid=39169f8f-4ab0-4f7b-9771-c3f7d0ddd61f&groupId=183920.

Herrera, Maria P.; Gómez-Martín, M. Esther; Medina, Josep R. (2017): Hydraulic stability of rock armors in breaking wave conditions. In *Coastal Engineering* 127, pp. 55–67. DOI: 10.1016/j.coastaleng.2017.06.010.

Hersbach, H.; Bell, B.; Berrisford, P.; Biavati, G.; Horányi, A.; Muñoz Sabater, J. et al. (2018): ERA5 hourly data on single levels from 1979 to present. Copernicus Climate Change Service (C3S) Climate Data Store (CDS). Available online at https://cds.climate.copernicus.eu/cdsapp#!/dataset/reanalysis-era5-single-levels?tab=overview, checked on (Accessed on 7/30/2020).

Hersbach, Hans; Bell, Bill; Berrisford, Paul; Hirahara, Shoji; Horányi, András; Muñoz-Sabater, Joaquín et al. (2020): The ERA5 global reanalysis. In *Q.J.R. Meteorol. Soc.* 146 (730), pp. 1999–2049. DOI: 10.1002/qj.3803.

Hoque, Md. Azharul; Perrie, William; Solomon, Steven M. (2020): Application of SWAN model for storm generated wave simulation in the Canadian Beaufort Sea. In *Journal of Ocean Engineering and Science* 5 (1), pp. 19–34. DOI: 10.1016/j.joes.2019.07.003.

Huong, N.T.T. (2003): SWAN prediction of nearshore wave climate at Nam Dinh coast in Vietnam. In *IHE MSc thesis 137*. Available online at https://repository.tudelft.nl/islandora/object/uuid:1e98c82b-7689-4e91-b75e-94acb39d2994?collection=research.

ICOE (2012): Geographic survey report - National scientific research: Study mechanisms of formation and development of coastal deposition in Ca Mau peninsular; propose scientific and technologic advance solutions for social and economic sustainable development. Code: ĐTĐL.2011-T/43. Báo cáo kết quả địa hình - Đề tài độc lập cấp nhà nước: Nghiên cứu cơ chế hình thành và phát triển vùng bồi tụ ven bờ và các giải pháp khoa học và công nghệ để phát triển bền vững kinh tế, xã hội vùng biển Cà Mau Mã số: ĐTĐL.2011-T/43. Institute of Coastal and Offshore Engineering (ICOE). Available online at https://sti.vista.gov.vn/tw/Pages/ket-qua-thnv.aspx?ItemID=52046&Type_CSDL=KETQUANHIEMVU&Keyword=2011-T/43&searchInFields=FullTextSM;Title&datasearch=&ListCoQuanChuQuan=&dsloai=&ListLinhVuc_Ma=.

ICOE (2017): National scientific research: Study of proper and technologic advance solutions to prevent coastal erosion, stabilize coastline of Mekong Delta, segment from Ca Mau peninsular to Ha Tien Code: ĐTĐL.CN-09/17. Nghiên cứu giải pháp hợp lý và công nghệ thích hợp phòng chống xói lở, ổn định bờ biển vùng đồng bằng sông Cửu Long, đoạn từ Mũi Cà Mau đến Hà Tiên. Mã số: ĐTĐL.CN-09/17.

Jordan, Christian; Tiede, Jan; Lojek, Oliver; Visscher, Jan; Apel, Heiko; Nguyen, Hong Quan et al. (2019): Sand mining in the Mekong Delta revisited - current scales of local sediment deficits. In *Scientific reports* 9 (1), p. 17823. DOI: 10.1038/s41598-019-53804-z.

Knapp, Kenneth R.; Diamond, Howard J.; Kossin, James P.; Kruk, Michael C.; Schreck, Carl J. (2018): International Best Track Archive for Climate Stewardship (IBTrACS) Project, Version 4.

Knapp, Kenneth R.; Kruk, Michael C.; Levinson, David H.; Diamond, Howard J.; Neumann, Charles J. (2010): The International Best Track Archive for Climate Stewardship (IBTrACS). In *Bull. Amer. Meteor. Soc.* 91 (3), pp. 363–376. DOI: 10.1175/2009BAMS2755.1.

Lappe, Ronja; Ullmann, Tobias; Bachofer, Felix (2022): State of the Vietnamese Coast—Assessing Three Decades (1986 to 2021) of Coastline Dynamics Using the Landsat Archive (Remote Sensing, 14).

Le Tu, Xuan; Thanh, Vo Quoc; Reyns, Johan; Van, Song Pham; Anh, Duong Tran; Dang, Thanh Duc; Roelvink, Dano (2019): Sediment transport and morphodynamical modeling on the estuaries and coastal zone of the Vietnamese Mekong Delta. In *Continental Shelf Research* 186, pp. 64–76. DOI: 10.1016/j.csr.2019.07.015.

Le Xuan, Tu; Le Manh, Hung; Ba, Hoang Tran; Van, Duong Do; Duong Vu, Hoang Thai; Wright, David et al. (2022): Wave energy dissipation through a hollow triangle breakwater on the coastal Mekong Delta. In *Ocean Engineering* 245, p. 110419. DOI: 10.1016/j.oceaneng.2021.110419.

Le Xuan, Tu; Tran Ba, Hoang; Le Manh, Hung; Do Van, Duong; Minh Nguyen, Nguyet; Wright, David P. et al. (2020): Hydraulic performance and wave transmission through pile-rock breakwaters. In *Ocean Engineering* 218, p. 108229. DOI: 10.1016/j.oceaneng.2020.108229.

Madden, Roland A.; Julian, Paul R. (1972): Description of Global-Scale Circulation Cells in the Tropics with a 40–50 Day Period. In *J. Atmos. Sci.* 29 (6), pp. 1109–1123. DOI: 10.1175/1520-0469(1972)029<1109:DOGSCC>2.0.CO;2.

Marchesiello, P.; San, D. C.; Hoang, T. B. (2017): Erosion processes in the Lower Mekong Delta Coastal Zones (LMDCZ) and measures for protecting Go-Cong and U-Minh from coastal erosion. Final report. Available online at http://www.siwrr.org.vn.

Marchesiello, Patrick; Nguyen, Nguyet Minh; Gratiot, Nicolas; Loisel, Hubert; Anthony, Edward J.; Dinh, Cong San et al. (2019): Erosion of the coastal Mekong delta: Assessing natural against man induced processes. In *Continental Shelf Research* 181, pp. 72–89. DOI: 10.1016/j.csr.2019.05.004.

Marchesiello, Patrick; San, Dinh Cong; Hoang, Tran Ba (2018): Erosion processes in the Lower Mekong Delta Coastal Zones and measures for protecting Go-Cong and Phu-Tan. Final Implementation Report. Edited by SOUTHERN INSTITUTE OF WATER RESOURCES RESEARCH (SIWRR). Agence Francaise de Development (AFD), European Union (EU), Southern Institute of Water Resources Research (SIWRR). Hi Chi Minh City. Available online at http://www.siwrr.org.vn.

MARD (2012): TECHNICAL STANDARDS FOR SEADIKE DESIGN: Issued in attachment with Decision No.1613/QD-BNN-KHCN dated July 9th, 2012 by the Ministry of Agriculture and Rural Development).

Minderhoud, P. S. J.; Coumou, L.; Erkens, G.; Middelkoop, H.; Stouthamer, E. (2019): Mekong delta much lower than previously assumed in sea-level rise impact assessments. In *Nature communications* 10 (1), p. 3847. DOI: 10.1038/s41467-019-11602-1.

Moghimi, Saeed; Gayer, Gerhard; Günther, Heinz; Shafieefar, Mehdi (2005): Application of third generation shallow water wave models in a tidal environment. In *Ocean Dynamics* 55 (1), pp. 10–27. DOI: 10.1007/s10236-005-0108-0.

Nguyen Trung Thanh; Karl Stattegger; Daniel Unverricht; Charles Nittrouer; Phung Van Phach; Paul Liu et al. (2017): Surface sediment grain-size distribution and sediment transport in the subaqueous Mekong Delta, Vietnam 39 (3). Available online at http://eprints.uni-kiel.de/41646/.

Nguyen, Nguyet-Minh; Dinh, Cong-San; Kim, Nguyen, Kim Dan; Pham, Quoc Bao; Gagnon, Alexandre S.; Mai, Son T.; Anh, Duong Tran (2022): Region of freshwater influence (ROFI) and its impact on sediment transport in the lower Mekong Delta coastal zone of Vietnam. Environmental Monitoring and Assessment 194, 463 (2022).

Nguyen, Nguyet-Minh; Dinh, Cong-San; Van-Duong, D.; Xuan-Tu, L.; Nestmann, F.; Zemann, M. et al. (2020): Evaluating the Effectiveness of Existing Coastal Protection Measures in Mekong Delta. In Nguyen Trung Viet, Dou Xiping, Tran Thanh Tung (Eds.): APAC 2019, vol. 175. Singapore: Springer Singapore, pp. 1419–1429.

Rogers, W. Erick; Kaihatu, James M.; Hsu, Larry; Jensen, Robert E.; Dykes, James D.; Holland, K. Todd (2007): Forecasting and hindcasting waves with the SWAN model in the Southern California Bight. In *Coastal Engineering* 54 (1), pp. 1–15. DOI: 10.1016/j.coastaleng.2006.06.011.

Takagi, Hiroshi; Thao, Nguyen Danh; Esteban, Miguel (2014): 1 - Tropical Cyclones and Storm Surges in Southern Vietnam. In Nguyen Danh Thao, Hiroshi Takagi, Miguel Esteban (Eds.): Coastal Disasters and Climate Change in Vietnam. Oxford: Elsevier, pp. 3–16. Available online at https://www.sciencedirect.com/science/article/pii/B9780128000076000010.

Takagi, Hiroshi; Thao, Nguyen Danh; Esteban, Miguel; Mikami, Takahito; van Cong; Thanh Ca, Vu (2015): Chapter 12 - Coastal Disasters in Vietnam. In Miguel Esteban, Hiroshi Takagi, Tomoya Shibayama (Eds.): Handbook of Coastal Disaster Mitigation for Engineers and Planners. Boston: Butterworth-Heinemann, pp. 235–255. Available online at https://www.sciencedirect.com/science/article/pii/B9780128010600000125.

Thanh, Vo Quoc; Reyns, Johan; Wackerman, Chris; Eidam, Emily F.; Roelvink, Dano (2017): Modelling suspended sediment dynamics on the subaqueous delta of the Mekong River. In *Continental Shelf Research* 147, pp. 213–230. DOI: 10.1016/j.csr.2017.07.013.

The Anh, Dao; van Tinh, Thai; Ngoc Vang, Nguyen (2020): The Domestic Rice Value Chain in the Mekong Delta. In Rob Cramb (Ed.): WHITE GOLD. The commercialisation of rice farming in the lower mekong basin. [Place of publication not identified]: SPRINGER Verlag, SINGAPOR, pp. 375–395.

The SWAN team (Ed.) (2018): Swan Technical documentation. SWAN Cycle III version 40.51. Delft University of Technology.

Thoai, Duong Thanh; Dang, Anh Nguyet; Kim Oanh, Nguyen Thi (2019): Analysis of coastline change in relation to meteorological conditions and human activities in Ca mau cape, Viet Nam. In *Ocean & Coastal Management* 171, pp. 56–65. DOI: 10.1016/j.ocecoaman.2019.01.007.

van den Brink, H. W.; Können, G. P. (2011): Estimating 10000-year return values from short time series. In *Int. J. Climatol.* 31 (1), pp. 115–126. DOI: 10.1002/joc.2047.

van der Linden, R.; Fink, A. H.; Zemann, M.; Nestmann, F. (2020): Comparison of Ocean Wave Data for Dimensioning of Coastal Protection Measures in the Vietnamese Mekong Delta Region. 100th AMS Annual Meeting. Boston, Massachusetts, USA, 2020. Available online at https://ams.confex.com/ams/2020Annual/meetingapp.cgi/Paper/365718.

van der Linden, Roderick; Fink, Andreas H.; Pinto, Joaquim G.; Phan-Van, Tan; Kiladis, George N. (2016): Modulation of Daily Rainfall in Southern Vietnam by the Madden–Julian Oscillation and Convectively Coupled Equatorial Waves. In *Journal of Climate* 29 (16), pp. 5801–5820. DOI: 10.1175/JCLI-D-15-0911.1.

Vu, Hoang Thai Duong; van Trinh, Cong; Tran, Dung Duc; Oberle, Peter; Hinz, Stefan; Nestmann, Franz (2021): Evaluating the Impacts of Rice-Based Protection Dykes on Floodwater Dynamics in the Vietnamese Mekong Delta Using Geographical Impact Factor (GIF). In *Water* 13 (9), p. 1144. DOI: 10.3390/w13091144.

Vu, Hoang Thai Duong; Zemann, Moritz; Oberle, Peter; Seidel, Frank; Nestmann, Franz (2022) Investigating Wave Transmission trough Curtain Wall Breakwaters under Variable Conditions. In Journal of Coastal and Hydraulic Structures, Vol. 2, 2022, paper 19. DOI: https://doi.org/10.48438/jchs.2022.0019.

Wheeler, Matthew C.; Hendon, Harry H. (2004): An All-Season Real-Time Multivariate MJO Index: Development of an Index for Monitoring and Prediction. In *Mon. Wea. Rev.* 132 (8), pp. 1917–1932. DOI: 10.1175/1520-0493(2004)132<1917:AARMMI>2.0.CO;2.